Research Article

Nitrate/Nitrite determination in water and soil samples accompanied by in situ azo dye formation and its removal by superabsorbent cellulose hydrogel

B. U. Gauthama[1] · B. Narayana[1] · B. K. Sarojini[2] · Kabiru Bello[2] · N. K. Suresh[1]

Received: 24 February 2020 / Accepted: 9 June 2020 / Published online: 16 June 2020
© Springer Nature Switzerland AG 2020

Abstract
In the present work, an efficient method is developed for the spectrophotometric determination of nitrite and nitrate ions in water and soil samples by in situ formation of azo dye (Griess reagent) which showed λ_{max} at 385 nm. The reaction condition and the concentration of reagents used are optimized. The molar absorptivity, Sandell's sensitivity, detection limit and quantification limit of the method are found to be 3.22×10^4 L mol^{-1} cm^{-1}, 1.98×10^{-6} µg cm^{-2}, 0.0030 µg mL^{-1} and 0.0092 µg mL^{-1} respectively with the linearity range up to 2.6 µg mL^{-1}. The formation of azo dye is confirmed by ^{1}H and ^{13}C Nuclear Magnetic Spectroscopy. The azo dye formed during the determination is effectively removed using custom made ecofriendly cellulose modified hydrogel in order to reduce organic load in the test samples. The structure, morphology and the thermal properties of hydrogel are determined by Fourier-transform infrared spectroscopy, scanning electron microscopy and thermogravimetric analysis respectively. The dye removal mechanism involves pseudo second order kinetics, adsorption is found to be spontaneous based on the thermodynamic parameters and it is befitting to Freundlich isotherm model.

Keywords Spectrophotometric · Nitrite · Nitrate · Adsorption · Hydrogel

1 Introduction

The bioaccumulation of nitrogenous pollutants like nitrite and nitrate in water and soil pose hazard to humans and plants. Nitrite is also utilized as an additive agent in food industry and its mishandle might lead to excessive amount of nitrite in consumables which is unwholesome to the public health. Organic nitrogen undergoes biochemical oxidation to form nitrate and can be readily converted into the more toxic nitrite by microbial reduction. The WHO recommends 6.5×10^{-5} M is to be the maximal allowed nitrite concentration in drinking water as per the norms of WHO [1].

Excess of nitrite in the aquatic ecosystem leads to the formation of algal blooms more and more which also the consequences of low oxygen level in the water, and it further leads to the increase in the temperature of that ecosystem leading to dead zone. Nitrite is an active ion in the nitrogen cycle, formed due to the imperfect oxidation of ammonia or reduction of nitrates. Nitrosamines are the potential carcinogen mostly formed due to nitrites [2]. Nitrite can enter the body as nitrate, can be converted into nitrite which effects the hemoglobin

Electronic supplementary material The online version of this article (https://doi.org/10.1007/s42452-020-3016-5) contains supplementary material, which is available to authorized users.

✉ B. Narayana, nbadiadka@gmail.com | [1]Department of Studies in Chemistry, Mangalore University, Mangalagangothri, Karnataka 574199, India. [2]Department of Industrial Chemistry, Mangalore University, Mangalagangothri, Karnataka 574199, India.

in delivering oxygen to the cells. A potentially fatal blue baby syndrome (*methemoglobinemia*)is also caused in infants due to nitrites. So, it is a major environmental concern, determination and removal of nitrite from water body has large scope [3, 4].

There are many methods and instrumental techniques such as polarography [5], voltammetry [6], fluorimetry [7], flow injection spectroscopy [8], bioamperometry [9], gas chromatography mass spectroscopy [10], kinetic methods [11, 12] described for the detection of nitrite, nitrate ions. But not all the methods are suitable for routine trace determination because some methods reported are either require expensive instruments or has complicated procedures. Thus, a utilization of above said methods is limited. On comparing with other methods spectrophotometric determination method gained more attention. Thus, highly sensitive, selective spectrophotometric method plays a significant role in the detection of nitrite and nitrate [13].

This spectrophotometric determination method is based on the Griess technique [14]. This involves the formation of diazonium salt from an aromatic primary amine, which is later couples with a coupling agent to form an azo dye which imparts colour to the solution. Nitrite ion in acidic medium gets converted into nitrous acid which catalyzes diazonium salt formation. Azo dye is a colour imparting material and the dye itself causes detrimental effects like intervening in the photosynthesis cycle of plants. It also has the affinity to generate carcinogenic/mutagenic products. The adsorption is the preferable method for the dye removal, since its relatively fast, appropriate and easy to carry out [15, 16].

Nature of adsorbent is the main effecting factor for the adsorption efficiency. Environmental safety, high adsorption capacity and low-cost productivity are the criteria for the ideal adsorbent. Biodegradable and biocompatible polysaccharide-based hydrogels induced interest in many researchers for testing them in application [17]. Hydrogel is the material which has an ability to absorb large amount of water in comparing with normal water absorbent material. They are insoluble in water and in most of the organic solvents which could be suitable for the liquid environment [18]. Their commendatory water sorption property makes them suitable for many fields such as cosmetics [19], sanitary napkins [20], tissue engineering [21], waste water treatment [22], biomedicine [23] and many more. Cellulose is the most available natural polymer at present, is one of the most ecofriendly non-dietary sources for the manufacture of variety of nature friendly materials such as paper products, biopolymers, biocomposites and so on. Notably its biodegradability, biocompatibility renewability and low preparation cost made researchers to focus more and more [24].

In the present study a method has been developed for the detection of nitrite and nitrate in water with high sensitivity, reproducibility with accuracy. Once the determination of nitrite and nitrate are carried out, the coloured solution which contains a hazardous organic pollutant dye was put into sewage without separation. To avoid this, present work involves the removal of dye using newly synthesized cellulose derived hydrogel namely poly (ATAC-co-NaAc) prepared using APS as initiator and MBA as crosslinker, grafted on the carboxy methyl cellulose backbone part. The optimized hydrogel was investigated for kinetics, isothermal and thermodynamic studies and adsorption–desorption studies in order to check the practicability of dye adsorption.

2 Materials and methods

2.1 Instrumentation

Spectrophotometric data were recorded using SHIMADZU UV-2550 double beam spectrophotometer (Shimadzu corporation, Japan) with 1 cm quarts cell. The infrared spectrum of the material was recorded on Bruker tensor 27 spectrophotometer. The functional group analysis of oven dried material was carried out using Attenuated Transmission Method with the frequency range of 400–4000 cm^{-1}. TGA analysis of the synthesized polymer was taken by thermogravimetric instrument (model: TGA 8000, Perkin Elmer). All samples (5–7 mg) injected with gas flow rate of 100 mL/min with heating rate of 10 °C/min at a temperature range of 25–600 °C under nitrogen atmosphere. Field emission scanning electron microscopy (FESEM) (JEOL 7600) was used for the determination of surface morphology of the CMC-g-poly (ATAC-co-NaAc). This sample analysis sputtered with gold up to 15 min and microgram were recorded at 15 kV accelerating current voltage. Nuclear Magnetic Resonance spectroscopy was used for the structural confirmation of synthesized dye and it was recorded in Bruker 400 MHz and 100 MHz for proton and carbon 13 spectra respectively.

2.2 Reagents and solutions used for spectrophotometric determination

Chemicals used were analytic grade, all solutions were prepared using double distilled water. $NaNO_2$ (0.1500 g) and KNO_3 (0.7200 g) were dissolved in water for the making of nitrite and nitrate solutions of 1000 µg mL^{-1} each in two different 100 mL standard flask respectively. Aqueous solutions of sulfanilic acid (0.5%), Resorcinol (0.5%), Hydrochloric acid (2.5 M), Sodium Hydroxide (2.5 M) and EDTA (2%) was prepared.

2.3 Materials used for the preparation of hydrogel

Ethanol and toluene used for the wax extraction were procured from Spectrochem India. For the cellulose extraction sodium hydroxide and sodium hypochlorite were used was obtained from Loba chem India. Ammonium persulfate (APS), isopropyl alcohol, acrylic acid, N, N-methylene-bis-acrylamide (MBA) and sodium monochloroacetate were obtained from Spectrochem India, whereas 3-acryloxyethyltrimethylammonium chloride (ATAC) and Sodium acrylate (SA) were obtained from Sigma Aldrich. Entire chemicals used were of analytical grade and were used as received without purification.

2.4 General procedure for the spectrophotometric detection of nitrite in water

To the series of 25 mL standard flask, added Aliquot of the nitrite sample of 0.2–30 µg mL^{-1}, added 1 mL each of sulfanilic acid and hydrochloric acid, shaken well for 2 min. Made to stand for 3 min at 0–5 °C for the diazotization reaction to conclude. Then added 1 mL each of resorcinol and sodium hydroxide. Distilled water used to make up to the mark. [25, 26]. The schematic representation was given in the Scheme 1.

2.5 General procedure for spectrophotometric detection of nitrate in water

Aliquot of nitrate of volume 10 mL was added to the beaker and added 5 mL conc. HCl and 2 g of granulated Zn/NaCl mixture, it was stirred at 30 rpm for 20 min to convert nitrate into nitrite. It was filtered through No. 41 Whatman filter paper to standard flask and diluted to 100 mL. Rest of the procedure was same as procedure for the detection of nitrite in water [27].

2.6 General procedure for detection of nitrate/nitrite in soil sample

To a clean 50 mL beaker, 1.0 g of soil sample was transferred. Then it was extracted using 0.5% sodium carbonate solution 4 times with 5 mL each, Whatman filter paper No. 41 was used for the filtration. Appropriate aliquots of the sample were transferred to 25 mL standard flask and analyzed for nitrite and nitrate according to the above procedure. All gave negative results. Now known amount of nitrite and nitrate were added separately, then analyzed using the same procedure.

2.7 General procedure for the Preparation of CMC-g-poly (ATAC-co-NaAc)

Graft copolymerization via free radical mechanism was performed for the making CMC-g-poly (ATAC-co-NaAc) on CMC. APS helped to initiate the reaction and role of MBA as cross linker. The main raw material i.e. CMC was made in our laboratory as reported [28], the preparation of performed via copolymerization of poly (ATAC-co-NaAc) on CMC using (APS) and (MBA) as initiator and cross linker respectively. In a typical reaction, 0.5 g of CMC was taken in a beaker containing 20 mL of distilled water with stirring for 10 h to get clear solution. Subsequently varied quantity of APS, ATAC and SA were added to the mixture with uniform stirring. Furthermore, different amount of MBA (0.01-0.120 g dissolved in 2 mL of demineralized water) was added and stirring continued for 3 h. Finally, the reactants were irradiated with 100-watt microwave power for 60 s for gelation. The hydrogel obtained was allowed overnight, followed by treated with three-fold of acetone for 3 h for the extraction of homopolymer. The unreacted monomers were removed by washing with distilled water [29]. It was then dried in an oven at 50 °C for 2 h and finally stored for further analysis. The percentage of grafting and its efficiency were evaluated using Eqs. (1) and (2) respectively.

Scheme 1 Schematic representation of preparation dye

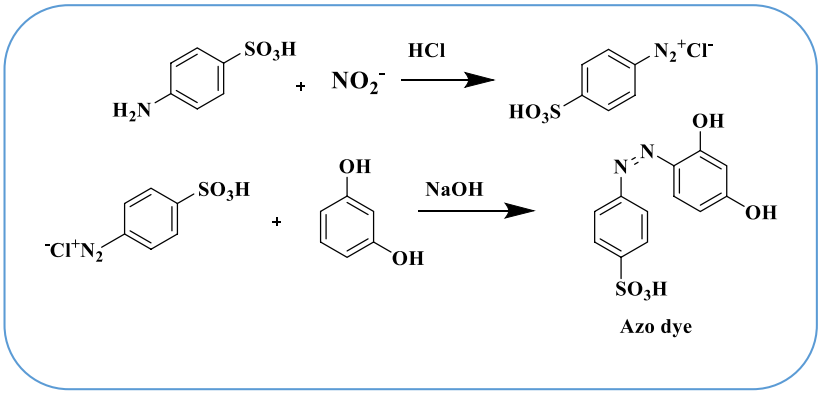

$$G.P. = \frac{W_2 - W_0}{W_0} \times 100 \quad (1)$$

$$G.E. = \frac{W_2 - W_1}{W_1} \times 100 \quad (2)$$

where W_0 is the weight of CMC, W_1 represents weight of (ATAC-co- NaAc) and W_2 represents CMC-g-poly (ATAC-co-NaAc) after the extraction of homopolymer. The schematic representation of the reaction was given in the Scheme 2.

2.8 General procedure for adsorption studies

A known quantity of CMC-g-poly (ATAC-co-NaAc) was placed in 200 mL of 100 mg L^{-1} dye solution. The solution was stirred for predetermined time at 100 rpm, at each time interval 3 mL of dye solution was taken out, centrifuged to remove solid particles and diluted to predefined concentration, analyzed in spectrophotometer. The sample were analyzed in the wave length range of 200–800 nm. The calibration curve and linear regression plot was obtained by converting λ_{max} of each sample into its concentration. The amount of dye adsorbed can be evaluated by the Eq. (3)

$$q_e = \frac{(C_o - C_e)}{M} \times V \quad (3)$$

where q_e (mg g^{-1}) represents the adsorption potential at equilibrium, C_o indicates initial dye concentration and C_e represents equilibrium dye concentration (mg L^{-1}) in aqueous solution, M (mg) and V (mL) represents the weight of the hydrogel and volume of dye solution taken respectively.

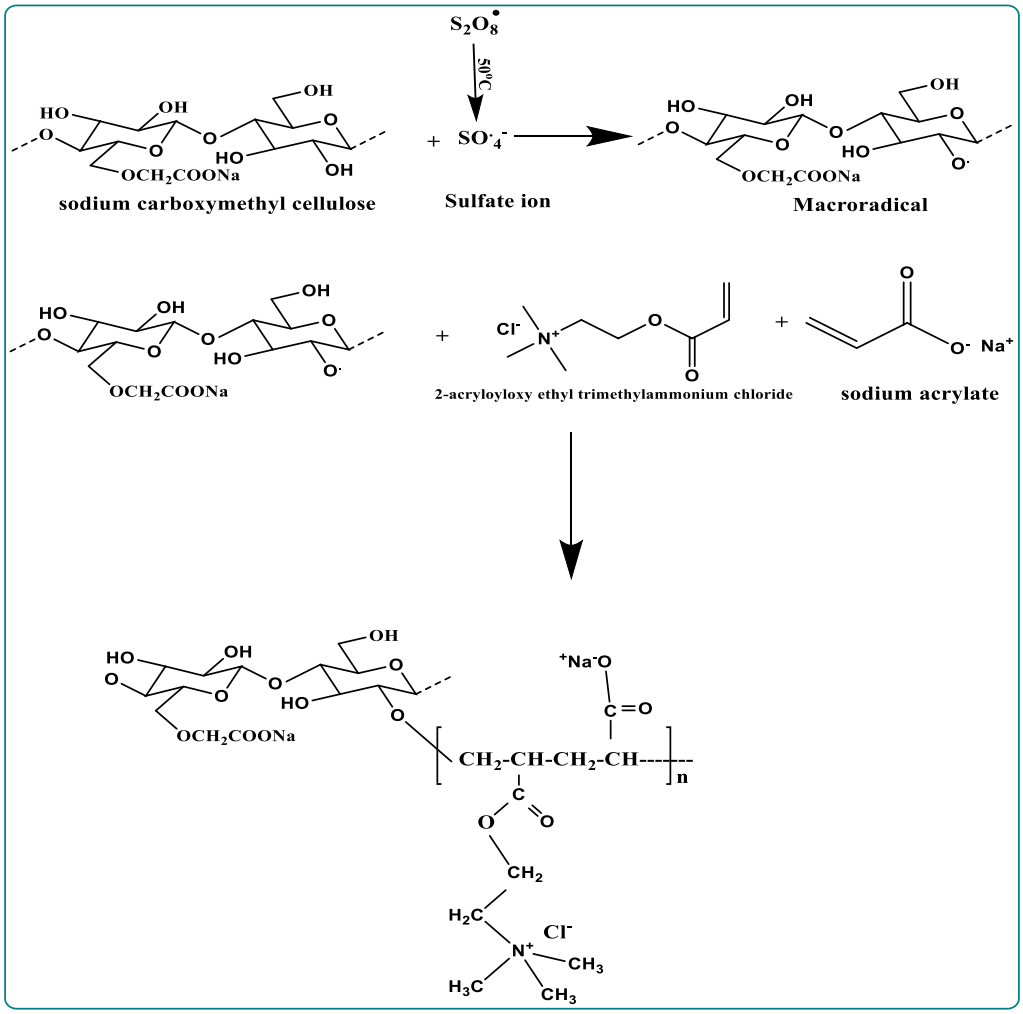

Scheme 2 Proposed reaction mechanism of CMC-g-poly (ATAC-co- NaAc)

2.9 General procedure for dye recycling studies

Dye adsorption–desorption investigation were performed out to check the reusability of the polymer. On the experiment, 100 mL of dye (isolated azo dye) solution of 100 mg L^{-1} was taken in a beaker to which added 17.4 mg of hydrogel and allowed it for adsorption up to its maximum adsorption of 3600 min. Later the hydrogel was removed from the solution and desorption experiment was proceeded. The adsorbed hydrogel was immersed in 0.5 mol L^{-1} each of HCl and NaOH solution, saturated NaCl solution of 100 mL each for 2 h at room temperature, hydrogel was taken out from the solution and washed with water to ensure hydrogel was free from dye on its surface, finally it was dried at 50 °C [30]. UV–Vis spectrophotometer was used to find out the amount of dye desorbed. The desorption ratio was calculated using the Eq. (4)

$$D\% = \frac{C_d V_d}{(C_o - C_e)V_i} \times 100 \quad (4)$$

where C_o was the initial concentration and C_e was the equilibrium concentration in the adsorbed solution whereas C_d was the dye concentration in the desorbed solution, V_i and V_d were the solution volume taken for adsorption and desorption respectively.

2.10 General procedure for the removal of azo dye from the real test samples

In order to remove the azo dye from the test samples, we used 2.6 µg mL^{-1} of nitrite test solutions as such with varied quantity of hydrogel to check the adsorption capacity of azo dye. Immediately after testing for nitrite and nitrate hydrogel was put into the test solutions for 20 h.

2.11 General procedure for the removal of excess of resorcinol

Since the dye formation involves resorcinol as a key raw material, there was a chance of presence of excess of resorcinol in the solution. The excess of unreacted resorcinol from the solution was removed by activated charcoal [31].

3 Results and discussions

3.1 Study of reagent concentration

The effect of variation of sulfanilic acid and resorcinol concentration on the colour intensity of the forming azo dye was studied using present method (Fig. S1 ESI*). From the study it was revealed that the volume of 1 mL of 0.5% each of sulfanilic acid and resorcinol solutions gave the maximum absorbance. A higher or lower concentration of the reagent showed less absorbance intensity and 1 mL each of both solutions was enough for the complete colour development.

3.2 Spectrophotometric study

The azo dye formed by the reaction of sulfanilic acid and resorcinol showed absorption maximum at 385 nm (Fig. 1a) in the spectrophotometer with the orange red colour. It was documented in the literature that the azo dye (was also called as Chrysoine resorcinol) exhibits absorption maximum at 387 nm evidencing the successful diazotization and coupling reactions [32]. Diazotization and coupling reaction were found to be temperature dependent and it should be carried at 0–5 °C and at 25 °C respectively. There were no distinguishable changes in the colour up to 35 °C. Above 40 °C there was a decrease in the intensity of colour of the solution. The reagents, 0.5% sulfanilic acid (1 mL), 0.5% resorcinol (1 mL), 2.5 M solution of both hydrochloric acid (1 mL) and sodium hydroxide (1 mL) solution per aliquot amount of sample 0.2–30 µg mL^{-1} resulted in maximum absorbance.

3.3 Validity of Beer–Lambert's law

By measuring the absorbance values of various concentration of nitrite solution ranging from 0.2 to 30 µg mL^{-1} (Fig. 1b). Beer's law was studied and results shows in the plot of absorbance versus concentration (Fig. 1c). From the plot it was evident that Beer's law obeyed from 0.2 to 2.6 µg mL^{-1} of nitrite. The molar absorptivity, Sandell's sensitivity, LOD ($D_L = 3.3\ \sigma/S$) and LOQ ($Q_L = 3.3\ \sigma/S$; where σ was the standard deviation of reagent blank (n = 5) and S was the slope of the calibration curve) of the method were 3.22×10^4 L mol^{-1} cm^{-1}, 1.98×10^{-6} µg cm^{-2}, 0.0030 µg mL^{-1} and 0.0092 µg mL^{-1} respectively which was compared to be better than the reference method developed earlier at our lab [25]. Comparison of final results obtained in present method with other cited methods are given in the Tables 1, 2a, b, 3.

3.4 Effect of interfering ions

The effect of diverse ions on the detection of nitrite/nitrate in the proposed method was studied with the fixed concentration of nitrite (2.6 µg mL^{-1}) and nitrate (2.6 µg mL^{-1}). The test result unveiled that Pb(II), Hg(II), Sn(II), Fe(III) found to interfere severely. The intensity of absorbance decreased substantially by the addition of

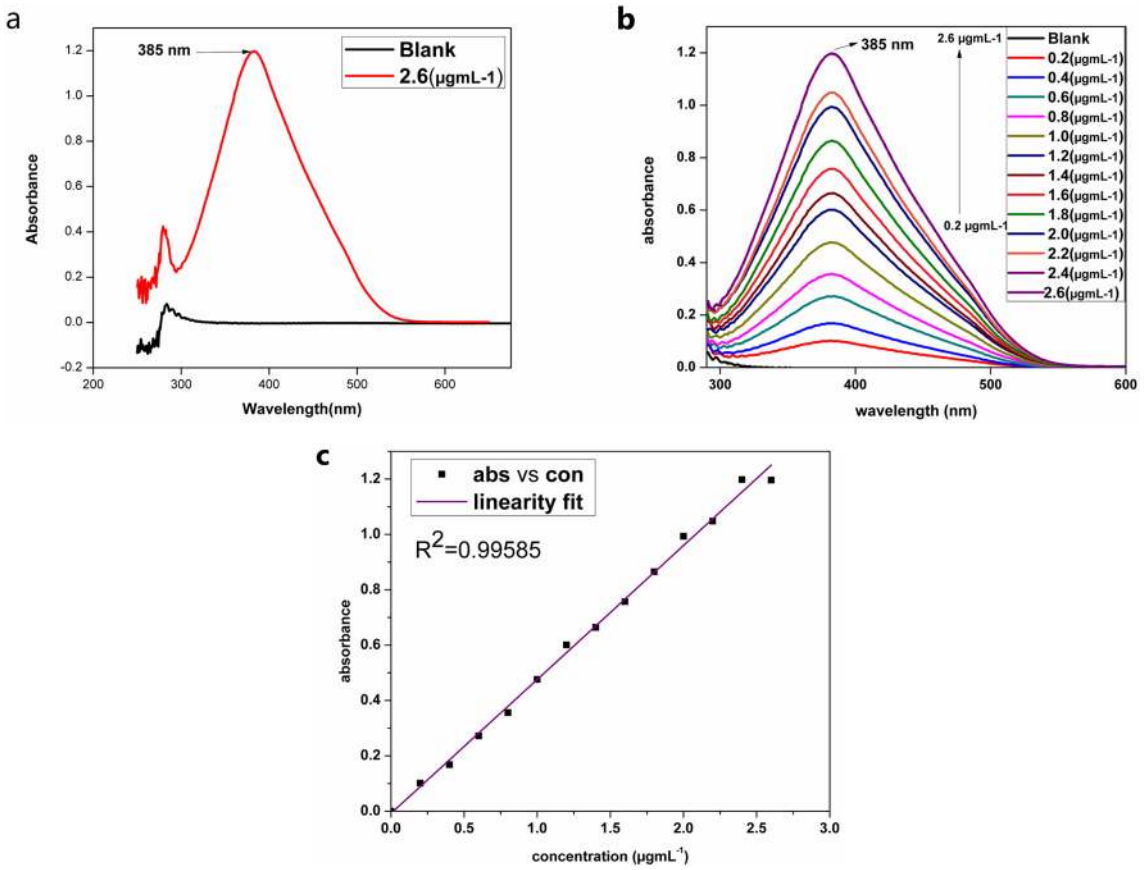

Fig. 1 **a** Absorption spectra of dye and reagent blank. **b** Absorption spectra at different concentrations. **c** Calibration curve

Table 1 Comparison of analytical data of proposed method with the other cited methods

Reagents used	Range μg mL^{-1}	Absorption maxima (nm)	Molar absorptivity L mol^{-1} cm^{-1}	Sandell's sensitivity μg cm^{-2}	LOD μg mL^{-1}	LOQ μg mL^{-1}	Reference no.
p-Nitro aniline-Frusmide	0.02–6.0	680	1.46×10^{3}	0.032	0.485	1.470	[13]
p-Nitro aniline-Ethyl acetoacetate	0.2–3.0	356	1.22×10^{4}	3.37×10^{-3}	–	–	[25]
p-Nitro aniline-Ethoxy ethylene maleic ester	0.2–18	439	5.04×10^{4}	0.98×10^{-2}	0.070	0.210	[26]
Sulfanilic acid-Methyl anthranilate	0.2–8.0	493	1.03×10^{4}	4.5×10^{-3}	0.930	2.820	[32]
Sulfanilic acid-Resorcinol	0.2–2.6	385	3.22×10^{4}	1.98×10^{-6}	0.0030	0.0092	Present method

these metal ions into the solution. The reaction of these metal ions with nitrite ions could be the reason for the early removal of nitrite ions from the solution thereby reducing the concentration of nitrite ions for diazotization. Anyhow, the tolerance limit of these ions was increased by adding 3 mL of 2% EDTA solution which preferentially chelates with these metal ions [42]. The tolerance limits of all tested ions are listed in the Table 4. The change in intensity of absorbance was not more than ± 2% caused by the change in the amount of targeted ions.

3.5 The NMR analysis for the confirmation of formation of azo dye

Structure of the dye, 4-((2,4-dihydroxyphenyl)diazinyl) benzenesulfonic acid) was confirmed by ^{1}H and ^{13}C NMR spectra (Fig. 2a, b). 1H NMR(400 MHz, DMSO–d_6): δ ppm,

Table 2 Tabulated values for the determination of nitrite in water (river, well and mineral) and soil samples

Sample	Nitrite added (μg mL^{-1})	Reference method [25]			Proposed method			[a]t-test	[b]F-test
		*Nitrite found (μg mL^{-1})	Recovery (%)	Relative error (%)	*Nitrite found (μg mL^{-1})	Recovery (%)	Relative error (%)		
a									
River water	1.0	0.992	99.2	0.80	0.996	99.6	0.70	1.70	1.76
	1.5	1.497	99.8	0.20	1.501	100.1	0.06	0.91	0.58
	2.5	2.495	99.8	0.20	2.498	99.9	0.08	0.99	1.71
Well water	1.0	0.994	99.4	0.60	0.995	99.5	0.50	0.87	1.50
	1.5	1.495	99.6	0.33	1.502	100.1	0.13	0.75	1.33
	2.5	2.498	99.9	0.08	2.497	99.8	0.12	1.12	1.22
Mineral water	1.0	0.997	99.7	0.3	0.998	99.8	0.20	1.10	1.51
	1.5	1.495	99.6	0.33	1.501	99.6	0.06	0.64	0.99
	2.5	2.496	99.8	0.16	2.497	99.8	0.12	0.90	1.11
Soil sample	0.8	0.798	99.7	0.25	0.798	99.7	0.25	1.99	0.87
	1.6	1.599	99.9	0.06	1.599	99.9	0.06	0.66	1.10
	2.4	2.393	99.7	0.29	2.402	100.1	0.08	1.29	1.33
Sample	Nitrate added (μg mL^{-1})	Reference method [25]			Proposed method			[a]t-test	[b]F-test
		*Nitrate found (μg mL^{-1})	Recovery (%)	Relative error (%)	*Nitrate found (μg mL^{-1})	Recovery (%)	Relative error (%)		
b									
River water	1.2	1.199	99.8	0.08	1.201	100.1	0.08	0.72	1.31
	1.8	1.792	99.6	0.44	1.797	99.8	0.16	1.72	1.36
	2.4	2.398	99.9	0.08	2.402	100.2	0.25	1.81	1.33
Well water	1.2	1.198	99.8	0.16	1.202	100.0	0.16	1.74	1.33
	1.8	1.793	99.6	0.38	1.797	99.8	0.16	1.12	1.12
	2.4	2.397	99.8	0.12	2.401	100.4	0.12	1.91	1.71
Mineral water	1.2	1.199	99.9	0.08	1.201	100.0	0.08	1.61	0.51
	1.8	1.794	99.6	0.33	1.798	99.8	0.11	1.51	1.14
	2.4	2.397	99.8	0.12	2.401	100.0	0.04	2.12	1.05
Soil sample	1.5	1.491	99.4	0.60	1.495	99.6	0.33	2.13	1.37
	2.0	1.983	99.2	0.85	2.006	100.3	0.35	2.20	1.20
	2.5	2.497	99.9	0.12	2.505	100.2	0.20	2.30	1.06

*Average of five determination

[a]Tabulated t-values for 5 degrees of freedom at 95% probability level is 2.015

[b]Tabulated F-values for (4,4) degrees of freedom at 95% probability level is 6.39

Table 3 Comparison of output data of proposed method with some electrochemical sensors

Sensing material	Analytical technique	LOD (μM)	References
MnO_2-CP-E	Linear Sweep voltammetry	1.2	[33]
Cobalt oxide	Cyclic voltammetry	20,000	[34]
CuO-graphite	Cyclic voltammetry	0.6	[35]
PbO_2-graphite	Cyclic voltammetry	0.9	[36]
f-ZnO@rFGO	Linear sweep voltammetry	33	[37]
$ZnTiO_3$-TiO_2	Amperometry	3.98	[38]
CuO-2TiO_2	Linear sweep voltametry	0.016	[39]
PEDOT/AUNCs	Amperometry	0.017	[40]
Bis(benzimazole)-Cu	Cyclivoltametry	0.22	[41]
Sulfanilic acid-resorcinol	Colorimtery	0.063	Present work

Table 4 Effect of diverse ions in the determination of nitrite (2.6μg mL^{-1}) and nitrate (2.6 μg mL^{-1})

Ions added	Tolerance limit (μg mL^{-1})	Ions added	Tolerance limit (μg mL^{-1})
Na^+	> 1000	Fluoride	1400
K^+	> 1000	Bromide	1400
Mg^{2+}	500	Iodide	1400
Ca^{2+}	500	Chloride	1000
Cd^{2+}	300	Citrate	800
Pb^{2+}*	75	Acetate	> 2000
Mn^{2+}	500	Oxalate	800
Ba^{2+}	250	Sulphate	1500
Hg^{2+}*	75	Phosphate	800
Sn^{2+}*	75		
$Al3^+$	400		
$Fe3^{+}$*	75		

*Masked by masked agent-2% EDTA solution

6.36 (s, 1H, Ar–H), 6.51 (d,1H, Ar–H), 7.65–7.85 (m, 5H, Ar–H), 10.62 (s, 1H, Ar–OH), 12.38 (s, 1H, Ar–OH), ^{13}C NMR (100 MHz, DMSO–d^6) 102.989 (C–N), 109.21 (C–N), 121.07, 126.66, 129.84, 132.34 (aromatic C's), 149.46 (CH), 150.36 (C–S), 156.53 (C–OH),163.17 (C–OH).

3.6 FT-IR analysis of hydrogel

Structural confirmation through functional groups identification of CMC and CMC-g-poly (ATAC-co-NaAc) was followed by FT-IR spectroscopy and its typical FTIR spectra were shown in the Fig. 3. IR spectra of CMC has all the normal peaks of cellulose includes peaks at 3332, 2914, 1626, 1026 cm^{-1} which were attributed to O–H, C–H, C=O, C–O stretching vibrations respectively. The same peaks observed in the backbone of CMC-g-poly (ATAC-co-NaAc). In addition to the above, CMC-g-poly (ATAC-co-NaAc) showed new peak at 1718 cm^{-1} corresponds to stretching vibrations of carbonyl groups of esters indicating the successful grafting [20]. The band at 1484 and 960 cm^{-1} corresponds to symmetric and asymmetric stretching vibrations of C–N bond in the 2-acryloxy ethyl trimethyl ammonium group which also another evident for the successful grafting. The one more evident for the successful grafting was shown by the peak at 1139 cm^{-1}, correlate with the C–O–C bond between carboxy cellulose back bone and alkyl group in the polymer [43].

3.7 FESEM analysis

Surface morphology of CMC and CMC-g-poly (ATAC-co-NaAc) were analyzed by FESEM. Figure 4 shows that CMC has a rod like shape whereas CMC-g-poly (ATAC-co-NaAc) surface morphology has completely different indicating successful grafting [44].

3.8 Thermogravimetric analysis

Thermogravimetric analysis was a complimentary technique from which one can get the idea about the composition and the thermal stability of the sample. Thermograms of the CMC and CMC-g-poly (ATAC-co-NaAc) were shown in the Fig. 5. It was integrated like, CMC has 3 stages of decomposition whereas CMC-g-poly (ATAC-co-NaAc) has 4 stages of decomposition with proportionate weight loss up on increase in the temperature. Both CMC and CMC-g-poly (ATAC-co-NaAc) dissipated initially from 25 to 91 °C and 25 to 70 °C with the loss in 10% and 4% mass respectively which might be due to loss disappearance of moisture content in the sample. There was insignificant decrease in weight on increase in temperature up to 280 °C for CMC. In addition, the second decomposition stage from 280 to 340 °C with 70% of total weight which may correspond to the decomposition of hydroxyl and carbonyl group of the polymer, similarly, third decomposition stage started from 340 °C till 500 °C with 20% weight loss. The CMC-g-poly (ATAC-co-NaAc) showed its second decomposition curve in the range of 250–290 °C with 30% loss in weight corresponded to the decomposition of carbonyl and hydroxyl groups. Third and its successive decomposition stage observed in the range of 350–400 °C with 20% weight loss and 450–550 °C with 15% of weight loss respectively. From the curve, it was concluded that CMC has lost its 70% of its weight below 340 °C whereas CMC-g-poly (ATAC-co-NaAc) lost only 30% of its weight indicating its significant higher thermal stability than the parent cellulose. It can also be considered as one of the evidences for successful grafting of CMC [45].

3.9 Adsorption kinetics

Kinetic study gives an important information about the adsorption mechanism of dye between the adsorbent and adsorbate which was necessary to predict the adsorbent adsorption rate and time, was given in the Fig. 6. The effect of contact time on the adsorption ability of CMC-g-poly with the dye. The adsorption of dye increased rapidly until reaching a constant value at a contact time of 3600 min. Pseudo first order (linear and nonlinear) and pseudo second order kinetics in the linear form were analyzed and were evidenced by Eqs. (5) and (6) respectively:

$$\log\left(q_e - q_t\right) = \log q_e - \frac{k_1}{2.303}t \quad (5)$$

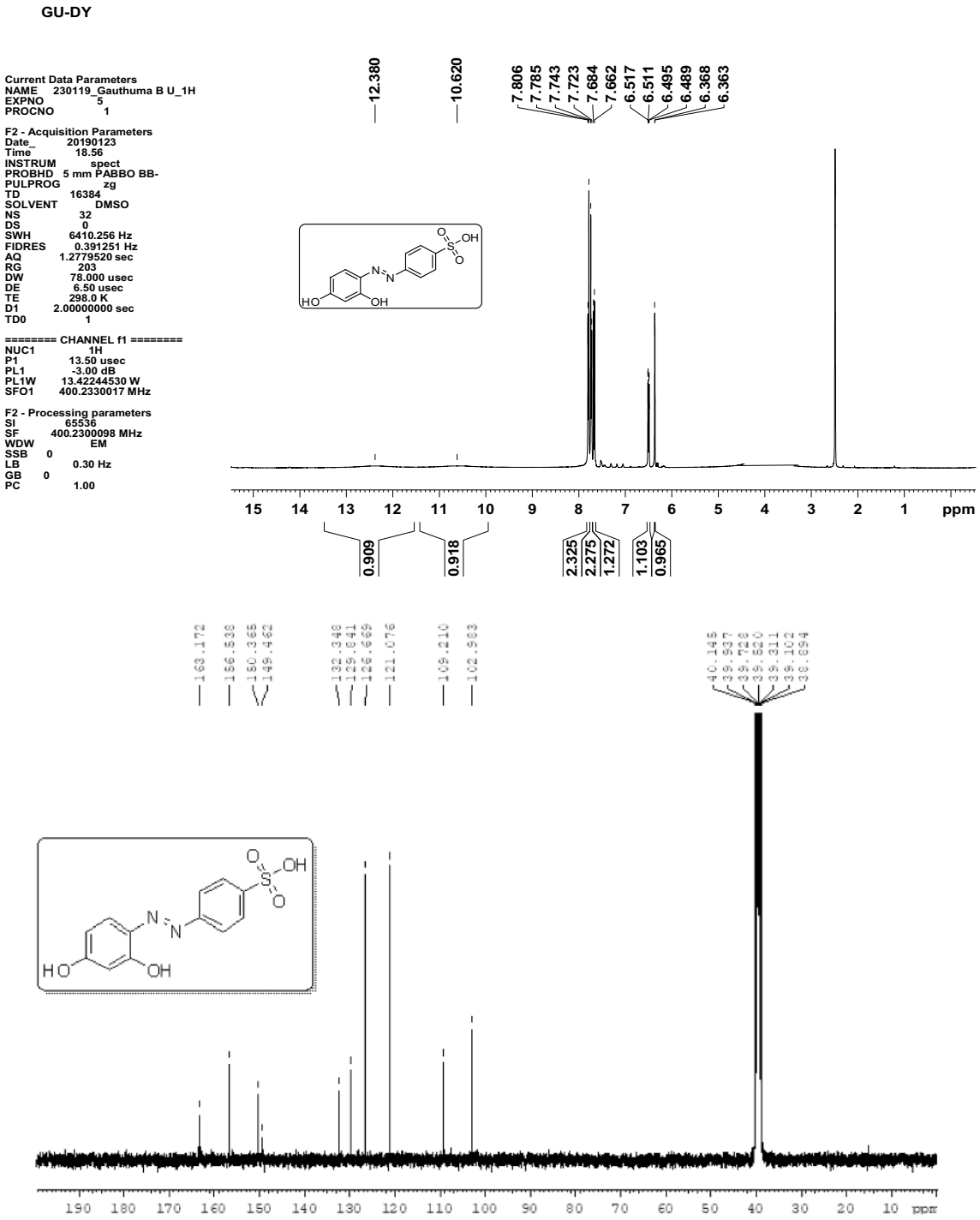

Fig. 2 **a** ^{1}H NMR of 4-((2,4-dihydroxyphenyl)diazinyl)benzenesulfonic acid), **b** ^{13}C NMR of 4-((2,4-dihydroxyphenyl)diazinyl)benzenesulfonic acid)

$$t/q_t = \frac{1}{k_2 q_e 2} + \frac{1}{q_e} \quad (6)$$

where k_1 and k_2 (g mg/min) are the rate constants, q_e (mg/g) was the amounts of dye adsorbed at equilibrium contact time and q_t (mg/g) was the adsorption at time t min, respectively.

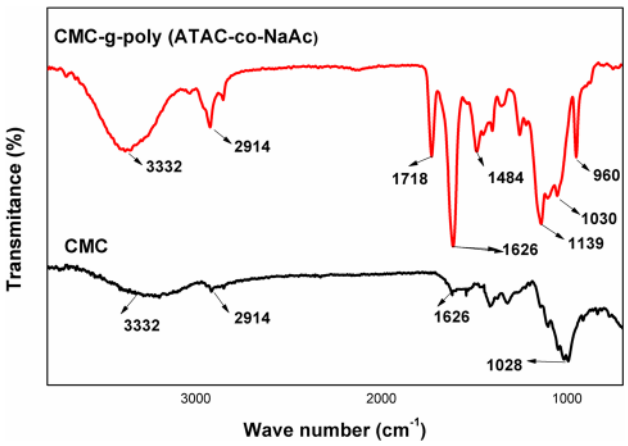

Fig. 3 FTIR spectra of graft copolymerized CMC-g-poly (ATAC-co-NaAc)

The correlation coefficient (R^2) for the pseudo-second (Linear) order kinetic model was 0.9811 and was considerably more than those of pseudo-second (Non-Linear) model and pseudo-first order model with correlation coefficient 0.8698 and 0.9562 (Table 5). This means the adsorption mechanism is chemisorption. Most importantly, theoretical amount of adsorption was near to the experimental values of pseudo second order kinetics [46–48].

3.10 Adsorption isotherm

Adsorption isotherm were predominant for discern the adsorbent-adsorbate interaction. Freundlich and Langmuir adsorption models were the two major, important models demonstrating the association between the adsorbent and adsorbate. Freundlich model gave empirical relation between the solute concentration on the adsorbent surface to the solute concentration in the medium whereas Langmuir model gives a relation between monolayer of adsorbate molecules surrounding a homogeneous solid surface called adsorbent. These two isotherm models were denoted by the Eqs. (7) and (8) respectively.

$$\frac{C_e}{q_e} = \frac{1}{q_m} C_e + \frac{K_L}{q_m} \tag{7}$$

$$\ln q_e = \ln K_F + \frac{1}{n} \ln C_e \tag{8}$$

where q_e (mg g^{-1}) was the amount of adsorbate at equilibrium adsorption and q_m was the amount of adsorbent adsorbed on saturated monolayer. The K_L and K_F were the constants of Langmuir and Freundlich models respectively and C_e (mg L^{-1}) was the dye concentration in solution at equilibrium. The heterogeneity factor 1/n or n represents adsorption intensity. From the plot of *log* q_e versus *log* C_e and C_e/q_e versus C_e, Freundlich and Langmuir adsorption models were demonstrated respectively (Fig. 7) [49].

It was evident that Freundlich isotherm model was fitted for the experimental value when compared with the Langmuir model since the correlation coefficient R^2 for Freundlich was 0.9962 on comparing with the correlation coefficient R^2 for Langmuir model. Freundlich adsorption isotherm model was depend on the hypothesis that adsorption was a multilayer process on the heterogeneous surface with irregular adsorption heat and affinity distribution [50]. If the n value was in between 1 and 10 then the adsorption was favorable and here it was 1.103. Remaining parameters were tabulated in the Table 6.

3.11 Adsorption thermodynamics

The adsorption rate and adsorption feasibility also depend on temperature of adsorption and it was evaluated by the thermodynamic specifications namely change in standard Gibb's free energy ΔG°, change in standard enthalpy ΔH° and change in standard entropy ΔS°. The spontaneity of

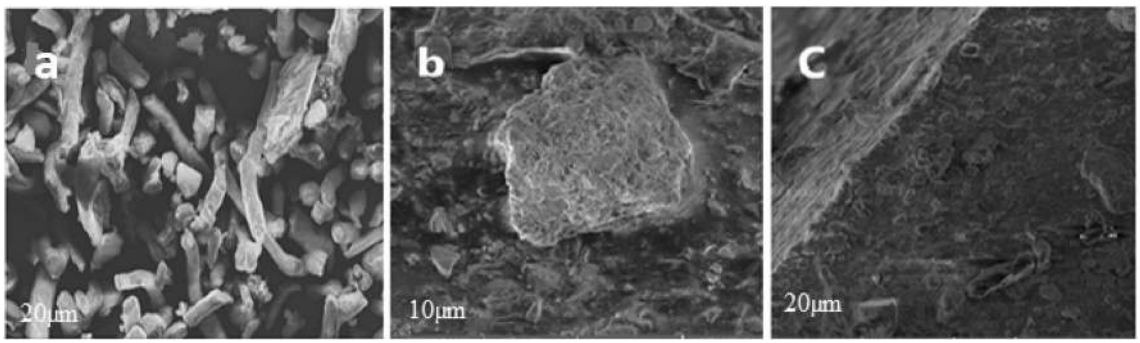

Fig. 4 SEM images of **a** CMC, **b** and **c** CMC-g-poly (ATAC-co-NaAc)

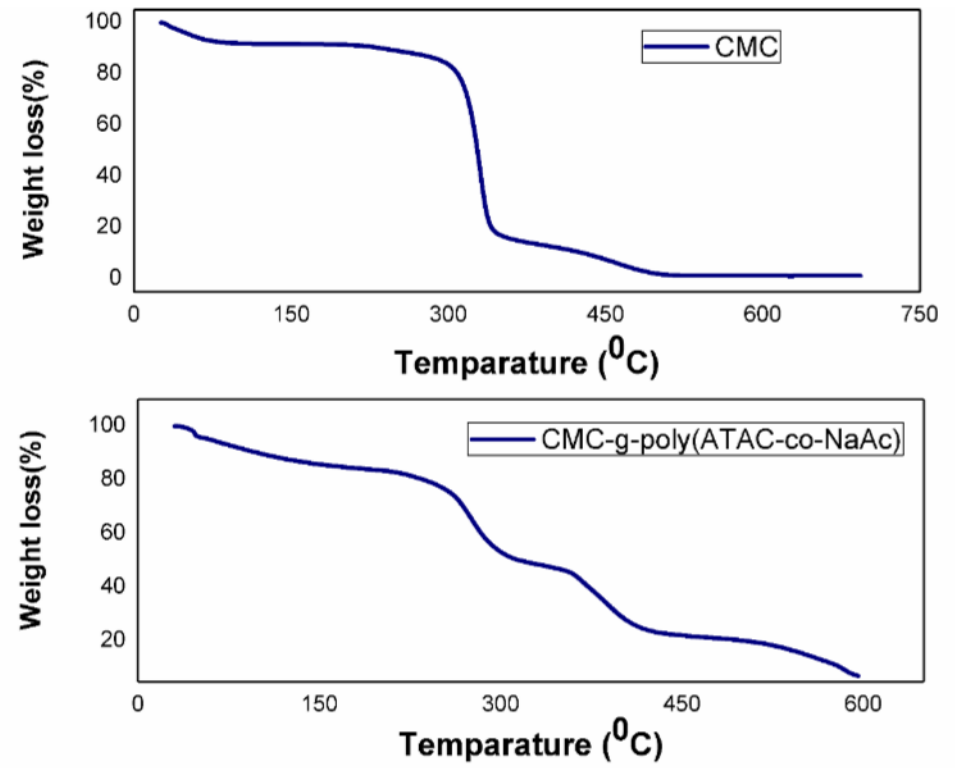

Fig. 5 TGA graph of CMC and CMC-g-poly (ATAC-co-NaAc)

adsorption depends on the Gibb's free energy and it was determined by the Eq. (9)

$$\Delta G^{o} = -RT \ln K \tag{9}$$

where K was thermodynamic equilibrium constant, R was the gas constant T was the temperature.

Thermodynamic constant K was affected by the change in temperature and it was given by the Eq. (10)

$$d\ln {}^{K}/_{dt} = \Delta H^{o}/RT \tag{10}$$

By integrating and on rearrangements of the Eq. (10), we get

$$\ln K = -\left(\frac{\Delta H^{o}}{RT}\right) + \frac{\Delta S^{o}}{R} \tag{11}$$

The change in the Gibb's free energy was given by

$$\Delta G^{o} = \Delta H^{o} - T\Delta S^{o} \tag{12}$$

ΔH° and ΔS° were determined from the intercept and slope of the graph lnK versus 1/T (Fig. 8). The calculated and theoretical thermodynamic parameters were reported in the Table 7. The positive value of ΔH° shows the adsorption process was endothermic in nature [51]. Theoretical and experimental Gibb's free energy value were approximately nearer which reflects that the adsorption was feasible with negative value indicating the spontaneous adsorption.

3.12 Recycling studies-adsorption and desorption

The recycling ability of the newly synthesized hydrogel was analyzed via continues adsorption–desorption process of dye. The stability of the hydrogel also studied by collecting the data of adsorption–desorption cycle. For the adsorption, solution of 100 mgL^{-1} of dye with hydrogel was stirred at room 28° C until the equilibrium adsorption achieved which was followed desorption studies. The desorption experiment was conducted at three different conditions i.e. acidic (0.5 M HCl solution), neutral (1% NaCl solution) and basic (0.5 M NaOH solution) pH. In the basic medium, adsorption–desorption cycle was restricted to one, this might be due to the nature of the hydrogel, the result shown in the Fig. S2 (ESI*). From the figure, it was evident that in acidic medium was favorable for the recycling over neutral

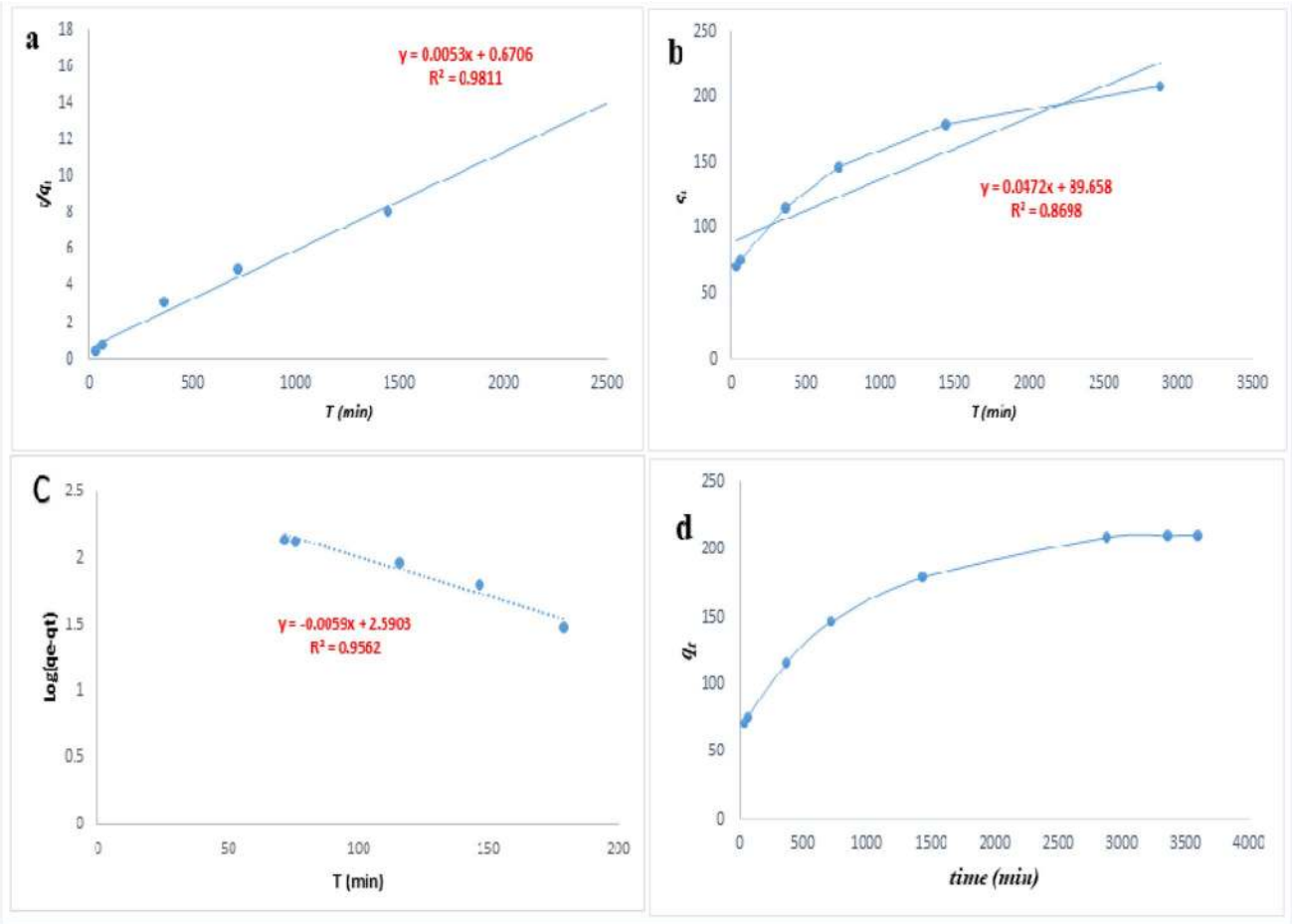

Fig. 6 **a** The pseudo second-order linear fit. **b** Pseudo second-order non-linear fit. **c** Pseudo first order adsorption kinetics for dye adsorption onto CMC-g-poly (APTAC-co-DMA; pH = 5–6, Dye concentrations = 100 mgL^{-1}, adsorbent dose = 76.5 mg 100 mL^{-1}). **d** Effect of contact time on adsorption of dye by CMC-g-poly(APTAC-co-DMA)

Table 5 Kinetic parameters for the adsorption of azo dye

Model	Kinetic parameter			
	$Q_{e, cal}$ (mg g^{-1})	K_1 (min^{-1})	R^2	$Q_{e, expt}$ (mg g^{-1})
Pseudo first order	389.30	1.35×10^{-2}	0.9562	208.65
Pseudo second order (Linear)	187.34	1.91×10^{-5}	0.9811	
Pseudo second order (Non-linear)	187.34	3.18×10^{-7}	0.8698	

medium and desorption experiment attained equilibrium in 1 h. Afterwards it was regenerated by drying at 50 ° C and reused for both adsorptive and desorptive studies. The adsorption–desorption cycle was carried out three times and there was a minimal decrease in the efficiency of hydrogel on multiple cycles. Therefore, the synthesized hydrogel has enough efficiency to use it several times with appreciable capacity [52–55].

3.13 Removal of dye from the test samples

Based on the above experiment, for the removal of azo dye from the test samples which was formed during the nitrite estimation, varied amount of hydrogel i.e. 20 mg, 40 mg and 70 mg were put into the test samples of 2.6 µg mL^{-1} of nitrite for 20 h. The results are shown in the Fig. S3 (ESI*). The figure shows that 20 mg and 40 mg of hydrogels

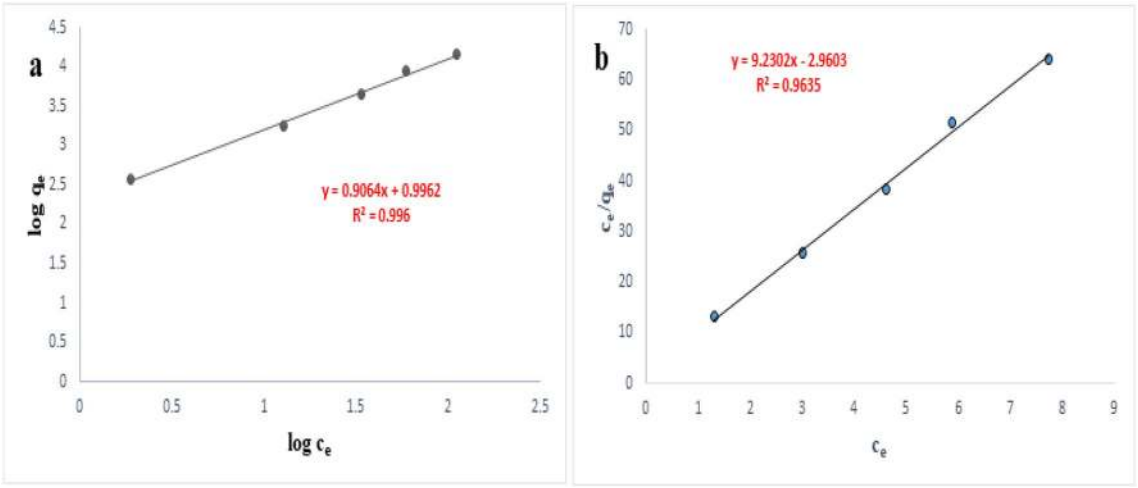

Fig. 7 **a** Freundlich. **b** Langmuir adsorption isotherms for the dye adsorption

Table 6 Langmuir and Freundlich adsorption isotherm coefficients for the adsorption of dye

Langmuir adsorption		Freundlich adsorption	
q_e (mg g^{-1})	0.108	n	1.103
K_L (L mg^{-1})	1.095×10^{-3}	KF	9.9265
R^2	0.9635	R^2	0.9962

were not adequate enough to remove azo dye completely whereas 70 mg of hydrogel was sufficient for the removal of 2.6 µg mL^{-1} azo dye completely.

3.14 Removal of surplus reagents

In the process of determining nitrite, resorcinol and sulfanilic acid were being used as reagents. There observed a peak of lesser intensity around 280 nm which could be attributed either resorcinol (λmax:273 nm) or sulfanilic acid (λ max: 290 nm) [56]. In order to remove these impurities, activated charcoal (100 mg) was added to the test sample priory treated with 70 mg of hydrogel and kept for equilibration for 12 h. The UV absorption spectrum depicted in Fig. S4 (ESI*) indicated absence of absorption peak (red line) attributing both for dye as well as impurities. Hence this was an attempt to detect nitrite/nitrate by in situ azo dye formation and removal of the pollutants and contaminants from the water body.

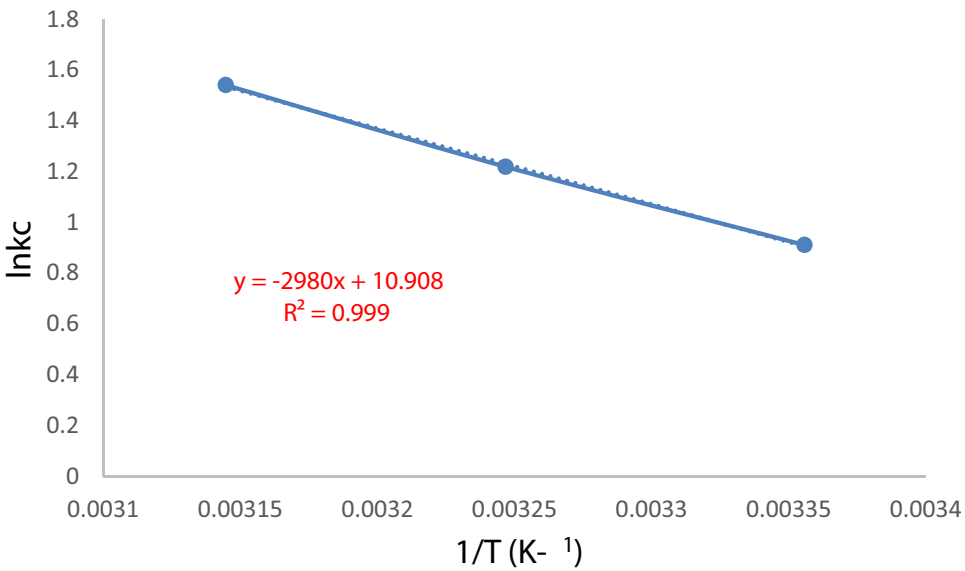

Fig. 8 Plot of ln K versus 1/T of adsorption of dye at different temperatures

Table 7 Thermodynamic parameters at variable temperatures

Temperature (K)	lnK	$\Delta G°$ (J/mol)		$\Delta H°$ (J/mol)	$\Delta S°$ (J/mol)
		Theoretical	Experimental		
298	0.9105	−2242.41	−2256.06	24,784	90.69
308	1.2184	−3149.33	−3120.17		
318	1.5401	−4056.26	−4071.80		

4 Conclusion

In summary, this paper presents an approach to determine the nitrite and nitrate present in soil and water with high sensitivity and selectivity using Griess reagent prepared by commercially available sulfanilic acid and resorcinol. This method of detection of nitrite and nitrate exhibits a wide linearity range and low detection limit compared to the previously reported results. In the determination process, the azo dye formed could be considered as secondary pollutant for the environment. Hence dye from the test solutions was effectively removed by adsorption using custom made ecofriendly superabsorbent hydrogel [graft copolymer CMC-g-poly (ATAC-co-NaAc)]. The 70 mg of the hydrogel successively removed dye with a concentration of 2.6 µg mL^{-1}. The dye removal mechanism involved pseudo second order kinetics, adsorption was found to be spontaneous based on the thermodynamic parameters and it was befitting to Freundlich isotherm model. In addition, the impurities like unreacted reagents resorcinol/sulfanilic acids were removed from the test solutions by equilibrating with activated charcoal for 12 h. Therefore, the present investigation uses the versatile Griess reagent to determine the primary pollutants effectively at the same time suggests an efficient method to remove secondary pollutant azo dye formed during the determination.

Acknowledgements The authors gratefully acknowledge BSR one time Grant to BN for purchase of chemicals. Authors thank DST-PURSE laboratory for TGA analysis and other facilities.

Author's contribution All authors have participated in this research, either by conception and design, or analysis and interpretation of the data; drafting the article or revising it critically for important intellectual content; and approval of the final version.

Compliance with ethical standards

Conflict of interest The authors declare that they have no conflict of interest.

References

1. Ren HH, Fan Y, Wang B, Yu LP (2018) Polyethylenimine-capped CdS quantum dots for sensitive and selective detection of nitrite in vegetables and water. J Agric Food Chem 66(33):8851–8858. https://doi.org/10.1021/acs.jafc.8b01951
2. Gürkan R, Altunay N (2018) Preconcentration and indirect quantification of trace nitrite, nitrate and total nitrite in selected beverage and milk samples using ion-pairing cloud-point extraction with acridine orange. J Food Compos Anal 69:129–139. https://doi.org/10.1016/j.jfca.2018.03.002
3. Wolff IA, Wasserman AE (1972) Nitrates, nitrites, and nitrosamines. Science 177(4043):15–19
4. Hetrick EM, Schoenfisch MH (2009) Analytical chemistry of nitric oxide. Ann Rev Anal Chem 2:409–433. https://doi.org/10.1146/annurev-anchem-060908-155146
5. Sabharwal S (1990) Determination of nitrite ion by differential-pulse polarography using N-(1-naphthyl) ethylenediamine. Analyst 115(10):1305–1307. https://doi.org/10.1039/AN9901501305
6. Van den Berg CM, Li H (1988) The determination of nanomolar levels of nitrite in fresh and sea water by cathodic stripping voltammetry. Anal Chim Acta 212:31–41. https://doi.org/10.1016/S0003-2670(00)84126-4
7. Diallo S, Bastard P, Prognon P, Dauphin C, Hamon M (1996) A new spectrofluorimetric microdetermination of nitrite in water after derivatization with 4-methyl-7-aminocoumarin. Talanta 43(3):359–364. https://doi.org/10.1016/0039-9140(95)01814-X
8. Chaurasia A, Verma KK (1994) Flow injection spectrophotometric determination of nitrite. Talanta 41(8):1275–1279. https://doi.org/10.1016/0039-9140(94)E0007-E
9. Jaim L (1993) Maria olimpia de oliveira rezende. Electroanalysis 5:251
10. Akyüz M, Ata Ş (2009) Determination of low level nitrite and nitrate in biological, food and environmental samples by gas chromatography–mass spectrometry and liquid chromatography with fluorescence detection. Talanta 79(3):900–904. https://doi.org/10.1016/j.talanta.2009.05.016
11. Nouroozi S, Mirshafian R (2009) Flow injection kinetic spectrophotometric method for the determination of trace amounts of nitrite. Talanta 79(4):1149–1153. https://doi.org/10.1016/j.talanta.2009.03.025
12. Kozub BR, Rees NV, Compton RG (2010) Electrochemical determination of nitrite at a bare glassy carbon electrode; why chemically modify electrodes. Sens Actuat B Chem 143(2):539–546. https://doi.org/10.1016/j.snb.2009.09.065
13. Veena K, Narayana B (2009) Spectrophotometric determination of nitrite using new coupling agents. http://hdl.handle.net/123456789/3216
14. Zimmermann K (1979) Analytical methods for nitrate and nitrite determination in foods. 3. Spectrophotometric determination of nitrate and nitrite using sulphanilic acid/1-naphylamine, and of nitrite using resorcinol/zirconium (IV) oxychloride. Die Nahrung 23(9–10):929–934
15. Khatri A, Peerzada MH, Mohsin M, White M (2015) A review on developments in dyeing cotton fabrics with reactive dyes for reducing effluent pollution. J Clean Prod 87:50–57. https://doi.org/10.1016/j.jclepro.2014.09.017
16. Kono H, Fujita S (2012) Biodegradable superabsorbent hydrogels derived from cellulose by esterification crosslinking with 1, 2, 3, 4-butanetetracarboxylic dianhydride. Carbohydr Polym 87(4):2582–2588. https://doi.org/10.1016/j.carbpol.2011.11.045
17. Crini G (2006) Non-conventional low-cost adsorbents for dye removal: a review. Bioresour Technol 97(9):1061–1085. https://doi.org/10.1016/j.biortech.2005.05.001

18. Soliman FM, Yang W, Guo H, Shinger MI, Idris AM, Hassan ES (2016) Preparation of carboxymethyl cellulose-g-poly (acrylic acid-2-acrylamido-2-methylpropane sulfonic acid)/attapulgite superabsorbent composite. Am J Polym Sci Technol 2(1):11–19. https://doi.org/10.11648/j.ajpst.20160201.12
19. Lee E, Kim B (2011) Smart delivery system for cosmetic ingredients using pH-sensitive polymer hydrogel particles. Korean J Chem Eng 28(6):1347. https://doi.org/10.1007/s11814-010-0509-8
20. Li Q, Ma Z, Yue Q, Gao B, Li W, Xu X (2012) Synthesis, characterization and swelling behavior of superabsorbent wheat straw graft copolymers. Bioresour Technol 118:204–209. https://doi.org/10.1016/j.biortech.2012.03.028
21. Chen Z, Wang W, Guo L, Yu Y, Yuan Z (2013) Preparation of enzymatically cross-linked sulfated chitosan hydrogel and its potential application in thick tissue engineering. Sci China Chem 56(12):1701–1709. https://doi.org/10.1007/s11426-013-4887-8
22. Souda P, Sreejith L (2014) Environmental sensitive hydrogel for purification of waste water: part 1: synthesis and characterization. Polym Bull 71(4):839–854. https://doi.org/10.1007/s00289-014-1097-2
23. Almomen A, Cho S, Yang CH, Li Z, Jarboe EA, Peterson CM, Huh KM, Janát-Amsbury MM (2015) Thermosensitive progesterone hydrogel: a safe and effective new formulation for vaginal application. Pharm Res 32(7):2266–2279. https://doi.org/10.1007/s11095-014-1616-8
24. Sun JX, Sun XF, Zhao H, Sun RC (2004) Isolation and characterization of cellulose from sugarcane bagasse. Polym Degrad Stab 84(2):331–339. https://doi.org/10.1016/j.polymdegradstab.2004.02.008
25. Sreekumar NV, Narayana B, Hegde P, Manjunatha BR, Sarojini BK (2003) Determination of nitrite by simple diazotization method. Microchem J 74(1):27–32. https://doi.org/10.1016/S0026-265X(02)00093-0
26. Cherian T, Narayana B (2006) A new system for the spectrophotometric determination of trace amounts of nitrite in environmental samples. J Braz Chem Soc 17(3):577–581. https://doi.org/10.1590/S0103-50532006000300022
27. Horita K, Wang G, Satake M (1997) Spectrophotometric determination of nitrate and nitrite in soil and water samples with a diazotizable aromatic amine and coupling agent using column preconcentration on naphthalene supported with ion-pair of tetradecyldimethylbenzylammonium and iodide. Anal Chim Acta 350(3):295–303. https://doi.org/10.1016/S0003-2670(97)00316-4
28. Bello K, Sarojini BK, Narayana B, Rao A, Byrappa K (2018) A study on adsorption behavior of newly synthesized banana pseudostem derived superabsorbent hydrogels for cationic and anionic dye removal from effluents. Carbohydr Polym 181:605–615. https://doi.org/10.1016/j.carbpol.2017.11.106
29. Soleimani F, Sadeghi H, Shahsavari H, Soleimani A, Sadeghi F (2013) Investigation of effective parameters onto swelling behaviour of superabsorbent hydrogels. Asian J Chem 25(9):4797–4800
30. Hakam A, Rahman IA, Jamil MSM, Othaman R, Amin MCIM, Lazim AM (2015) Removal of methylene blue dye in aqueous solution by sorption on a bacterial-g-poly-(acrylic acid) polymer network hydrogel. Sains Malays 44(6):827–834
31. Aghav RM, Kumar S, Mukherjee SN (2011) Artificial neural network modeling in competitive adsorption of phenol and resorcinol from water environment using some carbonaceous adsorbents. J Hazard Mater 188(1–3):67–77. https://doi.org/10.1016/j.jhazmat.2011.01.067
32. https://en.wikipedia.org/wiki/Chrysoine_resorcinol
33. Langley CE, Šljukic B, Banks CE, Compton RG (2007) Manganese dioxide graphite composite electrodes: application to the electroanalysis of hydrogen peroxide, ascorbic acid and nitrite. Anal Sci 23(2):165–170. https://doi.org/10.2116/analsci.23.165
34. Salimi A, Hallaj R, Mamkhezri H, Hosaini SMT (2008) Electrochemical properties and electrocatalytic activity of FAD immobilized onto cobalt oxide nanoparticles: application to nitrite detection. J Electroanal Chem 619:31–38. https://doi.org/10.1016/j.jelechem.2008.03.003
35. Šljukić B, Banks CE, Crossley A, Compton RG (2007) Copper oxide–graphite composite electrodes: application to nitrite sensing. Electroanal Int J Devot Fundam Pract Asp Electroanal 19(1):79–84. https://doi.org/10.1002/elan.200603708
36. Šljukić B, Banks CE, Crossley A, Compton RG (2007) Lead (IV) oxide–graphite composite electrodes: application to sensing of ammonia, nitrite and phenols. Anal Chim Acta 587(2):240–246. https://doi.org/10.1016/j.aca.2007.01.041
37. Pandikumar A, Yusoff N, Huang NM, Lim HN (2015) Electrochemical sensing of nitrite using a glassy carbon electrode modified with reduced functionalized graphene oxide decorated with flower-like zinc oxide. Microchim Acta 182(5–6):1113–1122. https://doi.org/10.1007/s00604-014-1436-x
38. Ehsan MA, Khaledi H, Pandikumar A, Rameshkumar P, Huang NM, Arifin Z, Mazhar M (2015) Nitrite ion sensing properties of $ZnTiO_3$–TiO_2 composite thin films deposited from a zinc–titanium molecular complex. New J Chem 39(9):7442–7452. https://doi.org/10.1039/C5NJ00850F
39. Ehsan MA, Naeem R, McKee V, Saeed AH, Pandikumar A, Huang NM, Mazhar M (2016) Electrochemical sensing of nitrite using a copper–titanium oxide composite derived from a hexanuclear complex. RSC Adv 6(33):27852–27861. https://doi.org/10.1039/C6RA00104A
40. Fan X, Lin P, Liang S, Hui N, Zhang R, Feng J, Xu G (2017) Gold nanoclusters doped poly (3, 4-ethylenedioxythiophene) for highly sensitive electrochemical sensing of nitrite. Ionics 23(4):997–1003. https://doi.org/10.1007/s11581-016-1865-0
41. Peng ZW, Yuan D, Jiang ZW, Li YF (2017) Novel metal-organic gels of bis (benzimidazole)-based ligands with copper (II) for electrochemical selectively sensing of nitrite. Electrochim Acta 238:1–8. https://doi.org/10.1016/j.electacta.2017.03.121
42. Narayana B, Sunil K (2009) A spectrophotometric method for the determination of nitrite and nitrate. Eurasian J Anal Chem 4(2):204–214
43. Dangge G, Xiying D, Chen C, Bin L, Jianzhong M (2015) Synthesis of polymer quaternary ammonium salt containing epoxy group/nanoZnO long-acting antimicrobial coating for cotton fabrics. Ind Eng Chem Res 54(43):10560–10567. https://doi.org/10.1021/acs.iecr.5b02509
44. Mahmoud GA, Mohamed SF, Hassan HM (2015) Removal of methylene blue dye using biodegradable hydrogel and reusing in a secondary adsorption process. Desalin Water Treat 54(10):2765–2776. https://doi.org/10.1080/19443994.2014.905978
45. Rusu AG, Popa MI, Lisa G, Vereştiuc L (2015) Thermal behavior of hydrophobically modified hydrogels using TGA/FTIR/MS analysis technique. Thermochim Acta 613:28–40. https://doi.org/10.1016/j.tca.2015.05.018
46. Mushtaq M, Bhatti HN, Iqbal M, Noreen S (2016) Eriobotrya japonica seed biocomposite efficiency for copper adsorption: isotherms, kinetics, thermodynamic and desorption studies. J Environ Manage 176:21–33. https://doi.org/10.1016/j.jenvman.2016.03.013
47. Borah L, Goswami M, Phukan P (2015) Adsorption of methylene blue and eosin yellow using porous carbon prepared from tea waste: adsorption equilibrium, kinetics and thermodynamics study. J Environ Chem Eng 3(2):1018–1028. https://doi.org/10.1016/j.jece.2015.02.013

48. Oladipo AA, Gazi M, Yilmaz E (2015) Single and binary adsorption of azo and anthraquinone dyes by chitosan-based hydrogel: selectivity factor and Box–Behnken process design. Chem Eng Res Des 104:264–279. https://doi.org/10.1016/j.cherd.2015.08.018
49. Wibowo E, Rokhmat M, Abdullah M (2017) Reduction of seawater salinity by natural zeolite (Clinoptilolite): adsorption isotherms, thermodynamics and kinetics. Desalination 409:146–156. https://doi.org/10.1016/j.desal.2017.01.026
50. El Qada EN, Allen SJ, Walker GM (2006) Adsorption of methylene blue onto activated carbon produced from steam activated bituminous coal: a study of equilibrium adsorption isotherm. Chem Eng J 124(1–3):103–110. https://doi.org/10.1016/j.cej.2006.08.015
51. Maneerung T, Liew J, Dai Y, Kawi S, Chong C, Wang CH (2016) Activated carbon derived from carbon residue from biomass gasification and its application for dye adsorption: kinetics, isotherms and thermodynamic studies. Bioresour Technol 200:350–359. https://doi.org/10.1016/j.biortech.2015.10.047
52. Malekbala MR, Khan MA, Hosseini S, Abdullah LC, Choong TS (2015) Adsorption/desorption of cationic dye on surfactant modified mesoporous carbon coated monolith: equilibrium, kinetic and thermodynamic studies. J Ind Eng Chem 21:369–377. https://doi.org/10.1016/j.jiec.2014.02.047
53. Oladipo AA, Ifebajo AO, Gazi M (2019) Magnetic LDH-based CoO–NiFe2O4 catalyst with enhanced performance and recyclability for efficient decolorization of azo dye via Fenton-like reactions. Appl Catal B 243:243–252. https://doi.org/10.1016/j.apcatb.2018.10.050
54. Chieng HI, Lim LB, Priyantha N (2015) Enhancing adsorption capacity of toxic malachite green dye through chemically modified breadnut peel: equilibrium, thermodynamics, kinetics and regeneration studies. Environ Technol 36(1):86–97. https://doi.org/10.1080/09593330.2014.938124
55. Ifebajo AO, Oladipo AA, Gazi M (2020) Sun-light driven enhanced azo dye decontamination from aqueous solution by CoO–CuFe. Desalin Water Treat 177(2020):423–430. https://doi.org/10.5004/dwt.2020.25247
56. Suresh S, Srivastava VC, Mishra IM (2011) Study of catechol and resorcinol adsorption mechanism through granular activated carbon characterization, pH and kinetic study. Sep Sci Technol 46(11):1750–1766. https://doi.org/10.1080/01496395.2011.570284

Publisher's Note Springer Nature remains neutral with regard to jurisdictional claims in published maps and institutional affiliations.